Argon spectral function and neutrino interactions

Artur M. Ankowski and Jan T. Sobczyk*
Institute of Theoretical Physics
University of Wrocław,
pl. Maksa Borna 9, 50-204 Wrocław, Poland
(Dated: February 7, 2008)

The argon spectral function is constructed and applied to neutrino-argon cross section computations in the plane wave impulse approximation with the Pauli blocking final state interaction effect taken into account. The approximations of the construction method are critically analyzed using the example of oxygen for which more detailed computations are available. An effective description of nucleus based on the information contained in a spectral function is proposed. It is demonstrated that its predictions are close to those obtained from the complete spectral function. The effective description can be easily applied in Monte Carlo event generators.

I. INTRODUCTION

In recent years, a lot of interest has been concentrated on improving the description of neutrino interactions [1]. The motivations behind this research are future precise neutrino experiments which require better knowledge about the cross sections. It also makes crucial whether the theoretical models can be implemented in Monte Carlo (MC) event generators.

Many papers focus on neutrino energies of a few GeV because this is the proposed energy range of several long-baseline experiments. In this energy region one has to consider both quasielastic and inelastic charge current (CC) processes. It is common to factorize neutrino-nucleus interaction into two steps: an interaction with a *single* bound nucleon (impulse approximation) and then reinteractions inside nucleus. The main difficulty is caused by the need of precise evaluation of the nuclear effects.

Existing MC codes rely on various versions of the Fermi gas (FG) model because it is straightforward to implement them in the MC routine. The simplest FG model with two adjustable parameters—Fermi momentum and average binding energy [2]—can be modified by inclusion of the recoil nucleus energy in the kinematics [3] and by local density effects [4]. It is, however, clear from the experience gained in describing the electron-nucleus interactions that the model can be considered only as the first approximation and that the MC simulations based on the FG model can be neither detailed nor precise.

The approach which introduces more realistic picture of a nucleus is the one using the spectral function (SF) [5]. The SF describes a distribution of momenta and removal energies of nucleons inside nucleus. In theoretical models, the SF combines contributions from the shell model (the mean field part) and from the short-range correlations. The second one (about 20% of the overall strength) accounts for the higher momentum and removal energy values [6, 7]. Recently, this part has been directly observed experimentally [8]. Computations based on the SF reproduce precisely the electron scattering data in the region of the quasielastic peak [9].

In this paper we adopt the plane wave impulse approximation (PWIA) and neglect the effects of final state interactions (FSI) except those from Pauli blocking. Evaluation of FSI is necessary in order to compare the predictions of the model with experimental data. It is argued in Refs. [9, 10] that in computation of the inclusive cross section (after summing over the final hadronic states) the construction of the SF and the treatment of FSI are two independent problems. Calculation of FSI effects is usually based on the complex optical potential. In the case of electron scattering, FSI do not change much the overall cross section at the fixed angle: the elastic peak is quenched and the cross section is redistributed making the peak wider. For the GeV neutrino interactions, i.e. when most of the quasielastic cross section corresponds to small values of Q^2, it is useful to distinguish Pauli blocking from the remaining FSI effects, because impact of the latter on the cross section is quite small (compare, for example fig. 14 in [9]).

There is a lot of discussion in the literature on the FSI effects in other approaches to quasielastic neutrino-nucleus scattering. In some of the recent papers (e.g., Ref. [11]), FSI is implied to be responsible only for a redistribution of the inclusive cross section among various exclusive observable channels. A similar meaning of FSI is adopted in many MC generators of events [1]. However in other theoretical approaches, the FSI effects modify also the inclusive cross section. In [12], it is achieved by using the dressed nucleon propagator with the contribution from the self-energy. References [13] and [14] describe the final nucleon wave function as a solution of the Dirac equation with the relativistic optical potential, the inclusive cross section is then obtained if the imaginary part of the potential is neglected. For 1 GeV neutrinos the FSI effects are reported to reduce the inclusive cross section by $\sim 10\%$.

*Electronic address: jsobczyk@ift.uni.wroc.pl

We confine our consideration to quasielastic reactions (the primary vertex), but we would like to stress that its extension to the resonance region is straightforward. Several papers consider the two dynamics together [11, 15], also in the formalism of the spectral function [16]. (Recent discussion of the resonance region can be found in [17, 18, 19].) However, we focus on the construction of the spectral function, and the inclusion of the resonance region is not likely to provide an extra input. In the discussion of the resonance region some new theoretical uncertainties appear: the properties of resonances in the nuclear matter and the nonresonant background [20]. It is well known that the theoretical understanding of the basic dynamics is still not complete since in the case of electron scattering it is difficult to reproduce the cross section in the dip region between the elastic and Δ resonance peaks [21].

For a few-GeV neutrino one has to consider also more inelastic channels. They are described by means of the DIS formalism with the specific techniques to include the nuclear effects. A recent comprehensive study discussed the following nuclear effects: Fermi motion and nuclear binding (FMB), off-shell corrections (OS), nuclear pion excess and coherent processes [22]. The results of the analysis show that in the kinematical region of large Bjorken x variable only FMB and OS effects are relevant. Both FMB and OS corrections are present in our approach: FMB is the core of the spectral function computations and OS were included in the de Forest prescription of evaluating weak current hadronic matrix elements [23].

There has been a lot of effort to calculate the spectral functions [6, 7, 24]. Systematic computations exist only for light nuclei up to oxygen and also for infinite nuclear matter. The aim of this paper is to calculate the spectral function for argon and to discuss its application to computation of the neutrino-argon cross section. Liquid-argon technology has been successively tested in the case of the ICARUS T600 module [25] and is now considered as an option in many neutrino experiments [26]. One of the experiments is the T2K where liquid-Ar detector is planned to be an element of the 2 km detector complex [27].

In our computations, we follow the approach proposed by Kulagin and Petti [22] which is partially based on the paper of Ciofi degli Atti and Simula [6]. The computations contain several approximations, and it is necessary to understand how precise the results are. For this reason we first analyze the approximation in the case of oxygen, the heaviest nucleus for which detailed computations of the spectral function exist. Our conclusion is that the agreement is satisfactory, and we pursue the computations for the argon.

Our paper is organized as follows. In Sec. II A we introduce basic definitions and formulas, Sec. II B shows how the spectral function corresponds to the Fermi gas model and in Sec. II C we present the approach of Kulagin and Petti [22]. In Sec. III A, we discuss in detail the predictions of the spectral function constructed for oxygen and compare them with the results obtained by Benhar *et al.* [9]. Most important are results contained in Secs. III B–III C. In Sec. III B we construct the argon spectral function. Then, having in mind implementations in MC event generators, in Sec. III C we investigate a procedure to extract an essential information contained in the spectral function. The information is encoded in two functions. The first one is the distribution of the nucleon momenta, and the second is the average binding energy for a given value of momentum. These two functions can be inserted in the Smith-Moniz formula for the inclusive cross section which can be easily implemented in a MC routine. Sec. IV contains the conclusions.

II. SPECTRAL FUNCTION IN PLANE WAVE IMPULSE APPROXIMATION

A. Neutrino-nucleus inclusive cross section

We denote the initial (final) lepton four-momentum as k (k') and the hadronic initial (final) four-momentum as p (p^f). In general, several hadrons or nuclei fragments can be in the final state $|f(p^f)\rangle$. The four-momentum transfer is $q \equiv (\omega, \mathbf{q}) \equiv k - k'$.

The neutrino-nucleus cross section is calculated in the Fermi theory approximation (in the neutrino energy range of a few GeV the condition $|q^2| \ll M_W^2$ is satisfied).

The inclusive neutrino-nucleus differential cross section reads:

$$\frac{d\sigma}{d^3k'} = \frac{G_F^2 \cos^2\theta_c}{8\pi^2 E_\nu E_\mu} L_{\mu\nu} W^{\mu\nu}, \tag{1}$$

where the leptonic tensor is defined as

$$
\begin{aligned}
L_{\mu\nu} &\equiv \frac{1}{4}\mathrm{Tr}[\gamma_\mu(1-\gamma_5)(\slashed{k}+m_l)\gamma_\nu(1-\gamma_5)(\slashed{k}'+m_l')] \\
&= 2(k_\mu k'_\nu + k'_\mu k_\nu - k\cdot k'\, g_{\mu\nu} - i\epsilon_{\mu\nu\rho\sigma}k^\rho k'^\sigma).
\end{aligned}
\tag{2}
$$

and the nuclear tensor is

$$
\begin{aligned}
W^{\mu\nu} &\equiv \overline{\sum_{f,i}}\langle f(p^f)|\mathcal{J}^\mu(0)|i(M_A)\rangle\langle f(p^f)|\mathcal{J}^\nu(0)|i(M_A)\rangle^* \\
&\times (2\pi)^6\delta^4(q+p_A-p^f),
\end{aligned}
\tag{3}
$$

It is convenient to express the cross section in terms of energy and momentum transfer:

$$\frac{d\sigma}{d\omega d|\mathbf{q}|} = \frac{G_F^2\cos^2\theta_C}{4\pi}\frac{|\mathbf{q}|}{E_\nu^2}L_{\mu\nu}W^{\mu\nu}. \tag{4}$$

In this paper we adopt PWIA, i.e. the approximation in which neutrino interacts with separate nucleons and the nucleon produced in the interaction leaves the nucleus without further reinteractions. We assume that

$$|f(p^f)\rangle = |R(p_R)\rangle \otimes |p'\rangle.$$

The spectral function $P(\mathbf{p}, E)$ is defined as the probability distribution to remove from the nucleus a nucleon with momentum $\mathbf{p}$ and leaving the residual nucleus with energy $E_R = M_A - M + E$:

$$P(\mathbf{p}, E) \equiv \overline{\sum_{R,\,i}} \delta(M_A - E_R - M + E)$$
$$\times \left| \langle R(p_R) | a(\mathbf{p}) | i(M_A) \rangle \right|^2. \qquad (5)$$

In our notation, $|i(M_A)\rangle$ is the state of the initial nucleus (assumed to be at rest) of mass M_A, $|R(p_R)\rangle$ is the final nucleus state (after a nucleon of momentum $\mathbf{p}'$ was ejected) of four-momentum $p_R = (E_R, \mathbf{p}_R)$, and M denotes the nucleon mass. Summation over all the final states and averaging over the spin states of the initial nucleus is performed. We omitted spin and isospin dependencies of the annihilation operator, but one has to keep in mind that there are two separate spectral functions: one for protons and another for neutrons.

The spectral function contains a lot of information about the nucleus. It follows from its definition that

$$n(\mathbf{p}) \equiv \int P(\mathbf{p}, E)\, dE = \overline{\sum_{R,\,i}} \left| \langle R(p_R) | a(\mathbf{p}) | i(M_A) \rangle \right|^2$$
$$= \overline{\sum_{i}} \langle i(M_A) | a^\dagger(\mathbf{p}) a(\mathbf{p}) | i(M_A) \rangle \qquad (6)$$

is the distribution of momenta inside the nucleus.

We normalize the nucleon distribution of momenta $n(\mathbf{p})$ (and then also the spectral function) as

$$\int d^3 p\, n(\mathbf{p}) = \int d^3 p\, dE\, P(\mathbf{p}, E) = \begin{cases} Z & \text{for protons,} \\ N & \text{for neutrons.} \end{cases} \qquad (7)$$

In PWIA it is straightforward to obtain the following expression for the inclusive cross section:

$$\frac{d\sigma}{d\omega d|\mathbf{q}|} = \frac{G_F^2 \cos^2\theta_C}{4\pi} \frac{|\mathbf{q}|}{E_\nu^2} \int dE\, d^3 p\, \frac{P(\mathbf{p}, E)}{E_\mathbf{p} E_{\mathbf{p}'}}$$
$$\times \delta(\omega + M - E - E_{\mathbf{p}'}) L_{\mu\nu} H^{\mu\nu}. \qquad (8)$$

where

$$H^{\mu\nu} = (2\pi)^6 \overline{\sum_{\text{spins}}} E_\mathbf{p} E_{\mathbf{p}'} \langle \mathbf{p}' | \mathcal{J}^\mu(0) | \mathbf{p} \rangle \langle \mathbf{p}' | \mathcal{J}^\nu(0) | \mathbf{p} \rangle^*$$
$$= \frac{M^2}{2} \text{Tr}\left(\Gamma^\mu \frac{\not{p} + M}{2M} \gamma_0 \Gamma^{\nu\dagger} \gamma_0 \frac{\not{p}' + M}{2M} \right) \qquad (9)$$

and

$$\Gamma^\mu = \gamma^\mu [F_1(q^2) + F_2(q^2)] - \frac{(p + p')^\mu F_2(q^2)}{2M}$$
$$+ \gamma^\mu \gamma_5 F_A(q^2) + \gamma_5 \frac{q^\mu F_P(q^2)}{M}. \qquad (10)$$

The hadronic tensor $H^{\mu\nu}$ has to be further specified because nucleons described by (9) are off shell. We will

adopt the standard de Forest prescription [23]: to approximate off-shell kinematics one can use free spinors and free form factors, taking into account that only a part of the energy is transferred to the interacting nucleon, and the rest is absorbed by the spectator system. It means that one makes a substitution

$$q = (\omega, \mathbf{q}) \to \widetilde{q} \equiv (\widetilde{\omega}, \mathbf{q}) \qquad (11)$$

where $\widetilde{\omega} = \omega - \overline{\epsilon}_B$, so that

$$H^{\mu\nu} \to \widetilde{H}^{\mu\nu} \qquad (12)$$

The model is finally specified by the form of the hadronic tensor:

$$\frac{H^{\mu\nu}}{M^2} = -g^{\mu\nu} H_1 + \frac{p^\mu p^\nu}{M^2} H_2 + i\varepsilon^{\mu\nu\kappa\lambda} \frac{p_\kappa q_\lambda}{2M^2} H_3$$
$$- \frac{q^\mu q^\nu}{M^2} H_4 + \frac{p^\mu q^\nu + q^\mu p^\nu}{2M^2} H_5 \qquad (13)$$

where

$$H_1 = F_A^2(1 + \tau) + \tau(F_1 + F_2)^2,$$
$$H_2 = F_A^2 + F_1^2 + \tau F_2^2,$$
$$H_3 = 2F_A(F_1 + F_2),$$
$$H_4 = \frac{1}{4} F_2^2(1 - \tau) + \frac{1}{2} F_1 F_2 + F_A F_P - \tau F_P^2$$
$$H_5 = H_2, \qquad (14)$$

with the notation $\tau = -q^2/(4M^2)$.

B. Fermi Gas model

In the FG model

$$P(\mathbf{p}, E) \propto \theta(p_F - |\mathbf{p}|) \qquad (15)$$

and one only has to decide about the way in which the energy is balanced.

In the previous section we used the energy conservation expressed as [compare the δ function in Eq. (3)]:

$$M_A + \omega = E_{\mathbf{p}'} + \sqrt{(M_{A-1})^2 + \mathbf{p}^2}. \qquad (16)$$

We recall that the initial nucleus state is assumed to be factorized into the neutron with momentum $\mathbf{p}$ and the spectator system with momentum $-\mathbf{p}$. The neutron energy can be written as

$$\sqrt{M^2 + \mathbf{p}^2} - \epsilon_B(\mathbf{p}) \equiv E_\mathbf{p} - \epsilon_B(\mathbf{p})$$

with binding energy $\epsilon_B(\mathbf{p}) \geq 0$, so that

$$M_A = \sqrt{(M_{A-1})^2 + \mathbf{p}^2} + E_\mathbf{p} - \epsilon_B(\mathbf{p}) \qquad (17)$$

and the energy conservation takes form

$$E_\mathbf{p} - \epsilon_B(\mathbf{p}) + \omega = E_{\mathbf{p}'}. \qquad (18)$$

The Smith–Moniz approach to the FG model [2] is to approximate $\epsilon_B(\mathbf{p})$ by the constant average value $\overline{\epsilon}_B$, that is,

$$E_{\mathbf{p}} - \overline{\epsilon}_B + \omega = E_{\mathbf{p}'}. \qquad (19)$$

The cross section calculated within this model (with Pauli blocking taken into account) is equal to

$$\begin{aligned}
\frac{d\sigma_{\text{S-M}}}{dE_\mu} &= \frac{G_F^2 \cos^2\theta_C}{4\pi E_\nu^2} \frac{3N}{4\pi p_F^3} \int d|\mathbf{q}|\, d^3p\, \theta(p_F - |\mathbf{p}|) \\
&\times \delta(\omega + E_{\mathbf{p}} - \overline{\epsilon}_B - E_{\mathbf{p}'})\, \theta(|\mathbf{p} + \mathbf{q}| - p_F) \\
&\times \frac{|\mathbf{q}|}{E_{\mathbf{p}} E_{\mathbf{p}'}} L_{\mu\nu} \widetilde{H}^{\mu\nu}.
\end{aligned} \qquad (20)$$

Using the concept of the spectral function one can say that the Smith-Moniz [2] version of the FG model is defined as

$$\begin{aligned}
P_{\text{S-M}}(\mathbf{p}, E) &= \mathcal{N}\delta(\sqrt{M^2 + \mathbf{p}^2} - \overline{\epsilon}_B - M + E) \\
&\times \theta(p_F - |\mathbf{p}|)
\end{aligned} \qquad (21)$$

where $\overline{\epsilon}_B$ is an average binding energy.

In the Bodek-Ritchie version of the FG model [3], one avoids the approximations in the energy delta function, obtaining

$$\begin{aligned}
P_{\text{B-R}}(\mathbf{p}, E) &= \mathcal{N}\delta(M_A - \sqrt{(M_{A-1})^2 + \mathbf{p}^2} - M + E) \\
&\times \theta(p_F - |\mathbf{p}|).
\end{aligned} \qquad (22)$$

In Ref. [3], the quadratic momentum distribution is modified by adding higher momentum tail. $\mathcal{N}$ is a normalization constant (the same in both cases).

In (21) and (22) Pauli blocking (PB) was ignored, because the usual PB term present in the expression for the cross section [i.e. $\theta(|\mathbf{p} + \mathbf{q}| - p_F)$] depends on the momentum transfer and therefore is not defined merely by characteristics of the nucleus. It is natural to treat it separately as a FSI effect.

C. Spectral function

In theoretical models, the SF consists of isoscalar and isovector parts [22]:

$$P(\mathbf{p}, E) = P_{\text{sc}}(\mathbf{p}, E) + P_{\text{vec}}(\mathbf{p}, E). \qquad (23)$$

It is common [9, 22, 28] to think of the isoscalar SF as itself consisting of two parts: the mean field (MF) and the short-range correlation parts, that is,

$$P_{\text{sc}}(\mathbf{p}, E) = \frac{N + Z}{2} \left[P_{\text{MF}}(\mathbf{p}, E) + P_{\text{corr}}(\mathbf{p}, E)\right], \quad (24)$$

with the normalization given by the condition

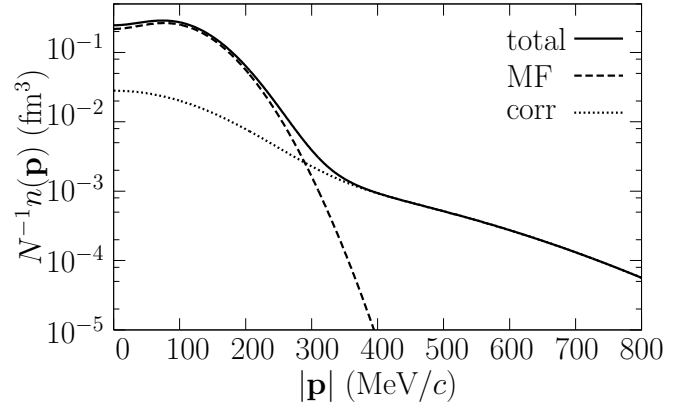$$\int dE\, d^3p\, \left[P_{\text{MF}}(\mathbf{p}, E) + P_{\text{corr}}(\mathbf{p}, E)\right] = 1. \qquad (25)$$

FIG. 1: Momentum distribution of nucleons in ^{16}O [6]. Dashed and dotted line shows the mean field and correlation contribution, respectively. The solid line represents their sum.

As a consequence, the momentum distribution (6) can also be represented as the sum of two contributions:

$$n(\mathbf{p}) = \frac{N + Z}{2} \left[n_{\text{MF}}(\mathbf{p}) + n_{\text{corr}}(\mathbf{p})\right]. \qquad (26)$$

Both $n_{\text{MF}}(\mathbf{p})$ and $n_{\text{corr}}(\mathbf{p})$ for a few nuclei are given in [6]. In Fig. 1 we see how they contribute to the overall momentum distribution of ^{16}O. These data will be used in the next section.

The mean field part $P_{\text{MF}}(\mathbf{p}, E)$ provides proper description of low-energy and low-momentum nucleons: they behave as Fermi gas in self-consistent mean field potential with energy levels given by the shell model. The presence of the correlation term $P_{\text{corr}}(\mathbf{p}, E)$ reflects the fact that in the ground state NN-correlations generate high momenta and high removal energies.

The low-energy contribution can be expressed as [29]

$$P_{\text{MF}}(\mathbf{p}, E) = \frac{1}{A} \sum_{\alpha < \alpha_F} A_\alpha n_\alpha(\mathbf{p}) \delta(E_\alpha + E_R(\mathbf{p}) - E) \quad (27)$$

with the recoil energy of the residual nucleus $E_R(\mathbf{p}) = \mathbf{p}^2/(2M_{A-1})$. In above equation $A = N + Z$ is the total number of nucleons, and A_α number of nucleons in the shell-model state α of energy E_α and momentum density distribution $n_\alpha(\mathbf{p})$ given by momentum space wave functions. In our convention, the values of E_α are positive below the Fermi level α_F.

When we replace E_α by the separation energy $E^{(1)}$ averaged over single-particle nucleon levels, the δ function can be taken outside the sum and the expression simplifies to [22]

$$\begin{aligned}
P_{\text{MF}}(\mathbf{p}, E) &= \delta(E^{(1)} + E_R(\mathbf{p}) - E) \frac{1}{A} \sum_{\alpha < \alpha_F} A_\alpha n_\alpha(\mathbf{p}) \\
&= n_{\text{MF}}(\mathbf{p})\, \delta(E^{(1)} + E_R(\mathbf{p}) - E).
\end{aligned} \qquad (28)$$

From $(e, e'p)$ experiments we know that (28) gives, in fact, only a part of $P(\mathbf{p}, E)$ because the depletion of

states is observed of a typical value ~ 0.2. It means that $\sim 20\%$ of the strength of the spectral function must be represented by a physics outside the shell model. It is usually explained in terms of short-range correlations producing pairs of high-momentum nucleons. To model $P_{\mathrm{corr}}(\mathbf{p}, E)$, one assumes that two nucleons form a cluster with high relative momentum and other $(A-2)$ nucleons remain soft [28]. Within this picture the following formula can be obtained [22]:

$$
\begin{aligned}
P_{\mathrm{corr}}(\mathbf{p}, E) \;=\; & n_{\mathrm{corr}}(\mathbf{p})\frac{M}{|\mathbf{p}|}\sqrt{\frac{\alpha}{\pi}} \\
& \times \left[\exp(-\alpha \mathbf{p}_{\min}^2) - \exp(-\alpha \mathbf{p}_{\max}^2)\right], \quad (29)
\end{aligned}
$$

where $\alpha = 3/(4\langle \mathbf{p}^2 \rangle \beta)$ with the mean square of momentum $\langle \mathbf{p}^2 \rangle$, $\beta = (A-2)/(A-1)$, and

$$
\begin{aligned}
\mathbf{p}_{\min}^2 &= \left[\beta|\mathbf{p}| - \sqrt{2M\beta[E - E^{(2)} - E_R(\mathbf{p})]}\right]^2, \\
\mathbf{p}_{\max}^2 &= \left[\beta|\mathbf{p}| + \sqrt{2M\beta[E - E^{(2)} - E_R(\mathbf{p})]}\right]^2.
\end{aligned}
\quad (30)
$$

The constant $E^{(2)}$ is the two-nucleon separation energy averaged over configurations of the $(A-2)$ nucleon system with low excitation energy.

Even in nuclei with equal number of neutrons N and protons Z there is a nonzero isovector contribution coming from Coulomb interaction and isospin-dependent effects in other interactions, but the standard approach is to neglect differences between the neutron and proton SF. Taking into account differences between the neutron and proton energy levels and their occupation probabilities in the approach presented here yields only small change of the threshold energy $E^{(1)}$, so it only slightly shifts the plot of the differential cross section. The reason of using the proton momentum distribution in both cases is purely practical: it's known with better accuracy.

For nonsymmetric nuclei, such as argon $^{40}_{18}\mathrm{Ar}$, the neutron SF must be different than the proton one. Due to the Pauli exclusion, the surplus neutrons can occupy only the Fermi level and thus it is assumed that the dominant contribution to $P_{\mathrm{vec}}(\mathbf{p}, E)$ comes from momenta and energies very close to the Fermi level. Kulagin and Petti [22] propose the approximation

$$
P_{\mathrm{vec}}(\mathbf{p}, E) = \frac{N-Z}{2}\frac{1}{4\pi \overline{p}_F^2}\,\delta(|\mathbf{p}| - \overline{p}_F)\delta(E - E_F). \quad (31)
$$

III. RESULTS

A. Verification of the method - an example of oxygen

It is important to check how good the presented approximation is for oxygen, for which detailed computation of the spectral function exists [9]. To perform the comparison we have to calculate the values of the constants appearing in (28) and (29): $E^{(1)}$, $E^{(2)}$, and $\langle \mathbf{p}^2 \rangle$.

TABLE I: Occupation probabilities c_{nl} [30] and numbers of particles $Z_{nl} = \frac{1}{2}A_{nl}$ for proton shell-model states in $^{16}\mathrm{O}$.

State	$^{16}\mathrm{O}$	Z_{nl}
$2s$	0.06	2
$1d$	0.14	10
α_F		
$1p$	0.80	6
$1s$	0.87	2

TABLE II: Energy spectrum of protons and neutrons in $^{16}\mathrm{O}$ [31] (the data for $1s_{1/2}$ and α_F are taken from [32]).

State α	Protons	Neutrons
$1d_{3/2}$	-4.65	-0.93
$2s_{1/2}$	0.08	3.27
$1d_{5/2}$	0.59	4.15
α_F		10
$1p_{1/2}$	12.11	15.65
$1p_{3/2}$	18.44	21.8
$1s_{1/2}$	45	47

One-nucleon separation energy $E^{(1)}$ has been introduced in (28) as an average energy of the single-particle states below the Fermi level, so

$$
E^{(1)} \;=\; \frac{1}{A}\sum_{\alpha < \alpha_F} A_\alpha E_\alpha \int n_\alpha(\mathbf{p})\,d^3 p = \frac{1}{A}\sum_{\alpha < \alpha_F} A_\alpha E_\alpha c_\alpha, \quad (32)
$$

where c_α is the occupation probability of the state α.

Multi-index α is a compact way of writing quantum numbers (nlj); therefore $A_\alpha \equiv A_{nlj}$, etc. The occupation probabilities c_{nlj} for oxygen $^{16}\mathrm{O}$ were not available to us, but we found values of c_{nl} defined as

$$
\begin{aligned}
c_{nl} \;&=\; \frac{2(l+\frac{1}{2})+1}{2(2l+1)}\,c_{nl(l+\frac{1}{2})} + \frac{2(l-\frac{1}{2})+1}{2(2l+1)}\,c_{nl(l-\frac{1}{2})} \\
&=\; \frac{l+1}{2l+1}\,c_{nl(l+\frac{1}{2})} + \frac{l}{2l+1}\,c_{nl(l-\frac{1}{2})}. \quad (33)
\end{aligned}
$$

It follows from the data for calcium in Sec. III B that the values of c_{nlj} for the levels differing only in spin state are very similar. Assuming that $c_{nl(l+\frac{1}{2})} \approx c_{nl(l-\frac{1}{2})}$ (or equivalently that $c_{nl(l-\frac{1}{2})} \approx c_{nl}$ and $c_{nl(l+\frac{1}{2})} \approx c_{nl}$) and using data from Tables I and II we get the following values:

$$
E^{(1)}_{^{16}\mathrm{O}} = 19.18 \text{ MeV for protons,}
$$

$$
E^{(1)}_{^{16}\mathrm{O}} = 22.32 \text{ MeV for neutrons.}
$$

The Benhar's spectral function was calculated for protons; therefore, to make appropriate comparisons, we used $E^{(1)}_{^{16}\mathrm{O}} = 19.18$ MeV in our numerical calculations. We checked also that applying the neutron value does not change the cross sections significantly.
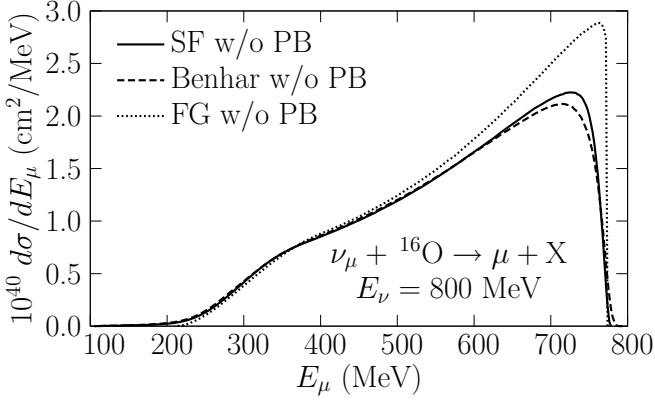
FIG. 2: Comparison of the quasielastic differential cross section $d\sigma/dE_\mu$ of ^{16}O for the Benhar's spectral function (dashed), our spectral function (solid), and the Fermi gas model with $p_F = 225$ MeV (dotted line). Pauli blocking is not included.
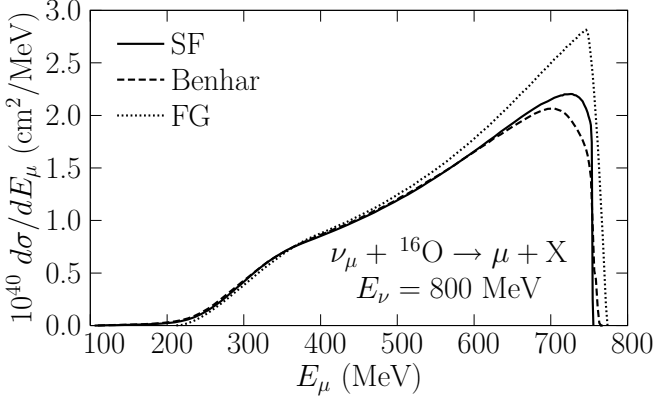

FIG. 3: Same as Fig. 2, but with Pauli blocking (details in the text).

Two-nucleon separation energy $E^{(2)}$ can be approximated by [22]

$$E^{(2)} = M_{A-2} + 2M - M_A, \tag{34}$$

and for oxygen we obtained

$$E^{(2)}_{^{16}\text{O}} = 26.33 \text{ MeV}.$$

The mean value of $\mathbf{p}^2$ is

$$\langle \mathbf{p}^2 \rangle \equiv \frac{\int \mathbf{p}^2 n_{\text{MF}}(\mathbf{p}) \, d^3 p}{\int n_{\text{MF}}(\mathbf{p}) \, d^3 p}. \tag{35}$$

Using the mean field momentum distribution for ^{16}O as in [6], we obtain

$$\langle \mathbf{p}^2 \rangle_{^{16}\text{O}} = \frac{3}{4}(\hbar c)^2 0.9 \text{ fm}^{-2} = (162.2 \text{ MeV}/c)^2.$$

Figure 2 shows a comparison of predictions for the oxygen differential cross section in energy transfer given by
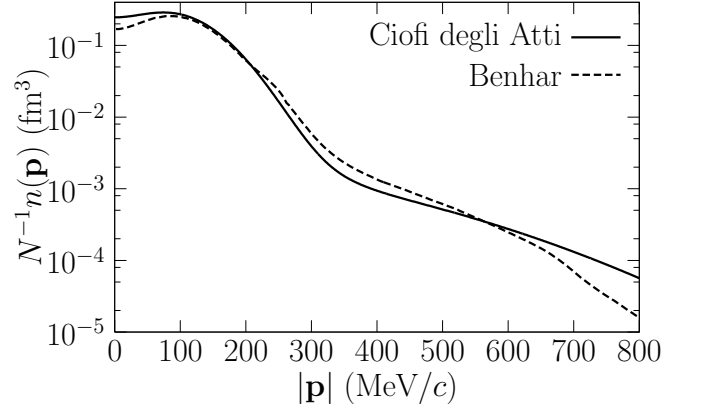

FIG. 4: Comparison of the nucleon momentum distribution computed from the Benhar's spectral function of ^{16}O and the distribution given by Ciofi degli Atti and Simula [6] used in our computations.
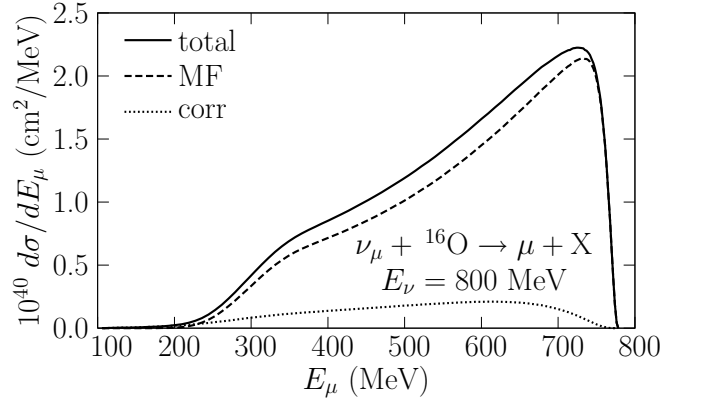

FIG. 5: Contributions to the quasielastic differential cross section $d\sigma/dE_\mu$ of ^{16}O in our spectral function with Pauli blocking ($\overline{p}_F = 209$ MeV). Mean field and correlation contribution are shown by dashed and dotted line, respectively. The solid line represents their sum.

our spectral function with predictions given by the Benhar's spectral function and the Fermi gas model. All numerical results in this paper have been obtained using the dipole parameterization of the form factors and axial mass $M_A = 1.03$ GeV.

To make comparisons with other numerical computations, we included the Pauli blocking effect, taking the *average* Fermi momentum calculated from the known density profile of a nucleus. The values we use are $\overline{p}_F = 209$ MeV [9] and $\overline{p}_F = 217$ MeV [33] for oxygen and argon, respectively. Note that the corresponding values needed for the FG model to reproduce the quasielastic peak in electron scattering [34] (namely, $p_F = 225$ MeV and $p_F = 251$ MeV) are visibly higher. We checked that the use of the same value for Pauli blocking in both FG and SF does not reduce discrepancy between them significantly.

The difference between predictions of two spectral

functions is not large, and it is greater if the Pauli blocking is included, see Fig 3. We identify two reasons why the discrepancy is observed. A part of it is explained by the different momentum distributions in the spectral functions (see Fig. 4). We deduce that the difference must be also caused by oversimplified treatment of the $P_{\mathrm{MF}}(\mathbf{p}, E)$, because for high E_μ this part gives dominant contribution to the differential cross section, as shown in Fig. 5.

In spite of simplicity of our approach, the results are in satisfactory agreement with the "exact" spectral function, and we continue our investigation to obtain a description of the argon nucleus.

TABLE III: Energy E_α, occupation probability c_α, and number of particles $Z_\alpha = \frac{1}{2}A_\alpha$ for proton shell-model states in $^{40}_{20}$Ca [35].

α	E_α	c_α	Z_α
$1g_{7/2}$	-21.00	0.04	8
$1g_{9/2}$	-9.75	0.06	10
$1f_{5/2}$	-4.51	0.08	6
$2p_{1/2}$	-2.02	0.07	2
$2p_{3/2}$	-0.92	0.08	4
$1f_{7/2}$	1.15	0.14	8
α_F	4.71		
$1d_{3/2}$	8.88	0.85	4
$2s_{1/2}$	10.67	0.87	2
$1d_{5/2}$	14.95	0.88	6
$1p_{1/2}$	31.62	0.91	2
$1p_{3/2}$	36.52	0.92	4
$1s_{1/2}$	57.38	0.93	2

TABLE IV: Energy E_α, occupation probability c_α, and number of particles $N_\alpha = \frac{1}{2}A_\alpha$ for neutron shell-model states in $^{40}_{20}$Ca [36].

α	E_α	c_α	N_α
$1f_{5/2}$	1.50	0.07	6
$2p_{1/2}$	4.19	0.07	2
$2p_{3/2}$	5.59	0.08	4
$1f_{7/2}$	8.54	0.12	8
α_F	12		
$1d_{3/2}$	15.79	0.89	4
$2s_{1/2}$	17.53	0.91	2
$1d_{5/2}$	22.48	0.93	6
$1p_{1/2}$	39.12	0.96	2
$1p_{3/2}$	43.8	0.96	4
$1s_{1/2}$	66.12	0.97	2

B. Argon spectral function

In nature, the most common isotope of argon is $^{40}_{18}$Ar. The feature of this nucleus which was not present in the previous calculations is its lack of isospin symmetry. It is obvious that for such nuclei, the vector contribution to
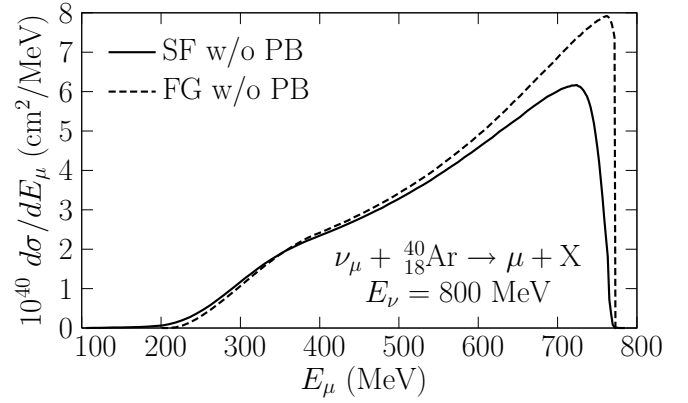

FIG. 6: Quasielastic differential cross section $d\sigma/dE_\mu$ off $^{40}_{18}$Ar as a function of produced muon energy E_μ for the Fermi gas model ($p_F = 251$ MeV, $\overline{\epsilon}_B = 28$ MeV) and the spectral function. Pauli blocking is absent.
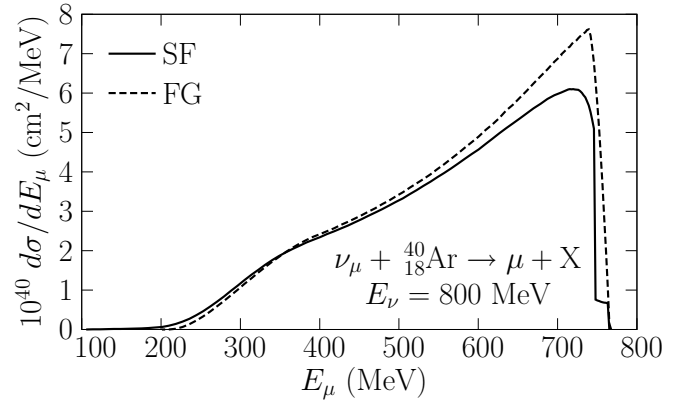

FIG. 7: Same as Fig. 6, but Pauli blocking is present.

the spectral function cannot be neglected, and therefore we estimate it using Eq. (31).

We lack data on the energy levels and occupation probabilities for the argon. The best we can do is to assume that they do not differ significantly from those for calcium given in Tables III and IV and use them to obtain the value of one-nucleon separation energy. In this way we get for neutrons

$$E^{(1)}_{^{40}_{18}\mathrm{Ar}} = 29.26 \text{ MeV}.$$

From Eq. (34) two-nucleon separation energy for argon is

$$E^{(2)}_{^{40}_{18}\mathrm{Ar}} = 16.46 \text{ MeV}.$$

We approximate the momentum distribution of argon with the one of calcium [6], what yields

$$\langle \mathbf{p}^2 \rangle_{^{40}_{18}\mathrm{Ar}} = \frac{3}{4}(\hbar c)^2 1.08 \text{ fm}^2 = (177.2 \text{ MeV})^2.$$

Using the argon spectral function, we calculated the inclusive cross section for neutrino-argon interaction
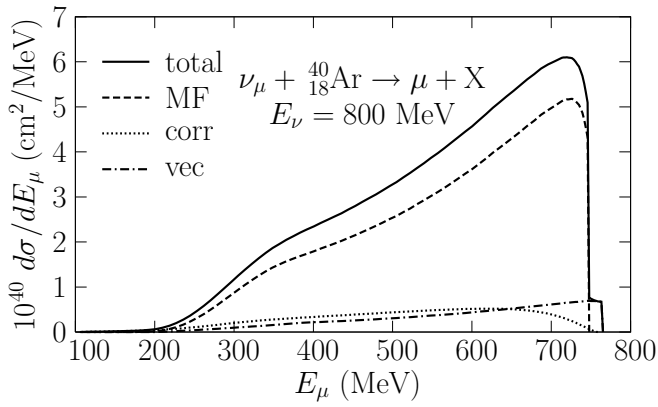
FIG. 8: Contributions to the differential cross section shown in Fig. 7 from $P_{\mathrm{MF}}(\mathbf{p}, E)$, $P_{\mathrm{corr}}(\mathbf{p}, E)$ and $P_{\mathrm{vec}}(\mathbf{p}, E)$.

first without (Fig. 6) and then with the Pauli blocking (Fig. 7). In Fig. 8, we show the contributions from $P_{\mathrm{vec}}(\mathbf{p}, E)$, $P_{\mathrm{MF}}(\mathbf{p}, E)$ and $P_{\mathrm{corr}}(\mathbf{p}, E)$. We see that $P_{\mathrm{vec}}(\mathbf{p}, E)$ is clearly responsible for the singular behavior of the differential cross section at small values of the energy transfer. The behavior at the quasielastic peak is determined mainly by the $P_{\mathrm{MF}}(\mathbf{p}, E)$ and the detail knowledge of argon energy levels can lead to modifications in this region. We also compared the differential cross section per neutron for oxygen and argon and found that they are rather similar.

C. Effective description of nucleus

Many Monte Carlo event generators rely on the Smith-Moniz version of the FG model despite the fact that the energy conservation given by Eq. (19) and the step-function momentum distribution provide a rather crude approximation of the real nucleus.

The use of the energy conservation written in (18) and the momentum distribution of a specific nucleus does not
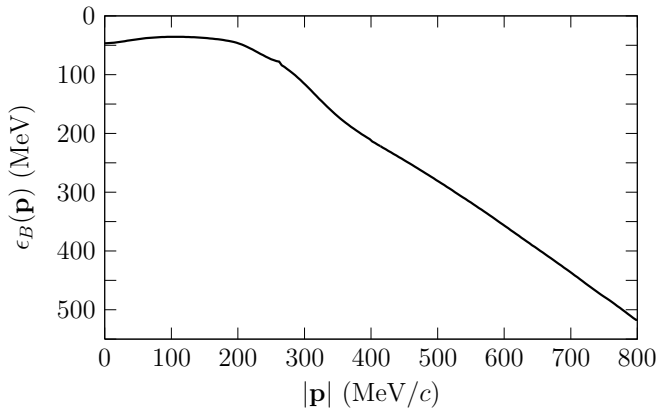

FIG. 9: Binding energy dependence on nucleon momentum $\epsilon_B(\mathbf{p})$ extracted from the Benhar's spectral function.
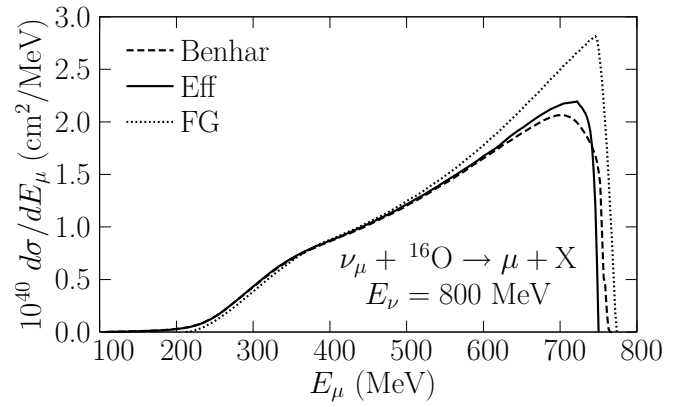

FIG. 10: Quasielastic differential cross section $d\sigma/dE_\mu$ off $^{16}\mathrm{O}$ obtained from the effective description, the Benhar's spectral function and the Fermi gas. Pauli blocking is present.

complicate model too much. This approach is simpler than the one based on the complete spectral function and is easy to apply in MC simulations. We refer to it as the *effective description*. It is defined by two functions $\epsilon_B(\mathbf{p})$ and $n(\mathbf{p})$ which characterize specific nucleus and can be calculated directly from the spectral function

$$n(\mathbf{p}) = \int dE P(\mathbf{p}, E)$$

and

$$\epsilon_B(\mathbf{p}) = \frac{1}{n(\mathbf{p})} \int dE \left(\sqrt{M^2 + \mathbf{p}^2} - M + E \right) P(\mathbf{p}, E). \quad (36)$$

The momentum distribution $n(\mathbf{p})$ obtained from the Benhar's spectral function for oxygen was presented in Fig. 4, and the binding energy dependence on momentum is shown in Fig. 9. One can see that high-momentum nucleons are deeply bound [29] and they cannot leave a nucleus. One can also see that for $|\mathbf{p}| \in [0; 200]$ MeV, the binding energy is roughly constant, varying between ~ 35 and ~ 47 MeV.

The cross section in the effective description is of the form

$$\begin{aligned} \frac{d\sigma_{\mathrm{eff}}}{dE_\mu} &= \frac{G_F^2 \cos^2 \theta_C}{4\pi E_\nu^2} \frac{N}{\int d^3 p\, n(\mathbf{p})} \int d|\mathbf{q}|\, d^3 p\, n(\mathbf{p}) \\ &\times \delta\left(\omega + E_\mathbf{p} - \epsilon_B(\mathbf{p}) - E_{\mathbf{p}'}\right) \theta(|\mathbf{p} + \mathbf{q}| - \overline{p}_F) \\ &\times \frac{|\mathbf{q}|}{E_\mathbf{p} E_{\mathbf{p}'}} L_{\mu\nu} \widetilde{H}_{\mathrm{eff}}^{\mu\nu}. \end{aligned} \quad (37)$$

The only difference between $L_{\mu\nu} \widetilde{H}_{\mathrm{eff}}^{\mu\nu}$ and $L_{\mu\nu} \widetilde{H}_{\mathrm{S\text{-}M}}^{\mu\nu}$ lies in the energy transfer, because now $\widetilde{\omega} = \omega - \epsilon_B(\mathbf{p})$.

Figs. 10–14 show results obtained within this model.

The effective description of oxygen makes use of the Benhar's spectral function. The cross section $d\sigma_{\mathrm{eff}}/dE_\mu$ (Fig. 10) is only slightly different with respect to the one calculated with the spectral function. The difference is seen at low energy transfer. We notice that the effective
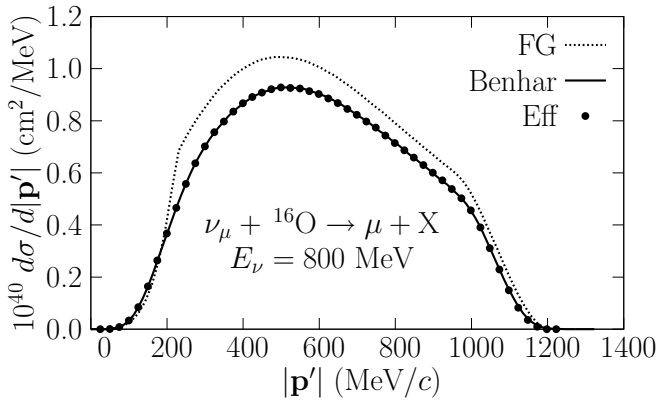
FIG. 11: Quasielastic differential cross section $d\sigma/d|\mathbf{p}'|$ off ^{16}O obtained from the effective description, the Benhar's spectral function and the Fermi gas ($p_F = 225$ MeV, $\overline{\epsilon}_B$=27 MeV). Pauli blocking is absent.
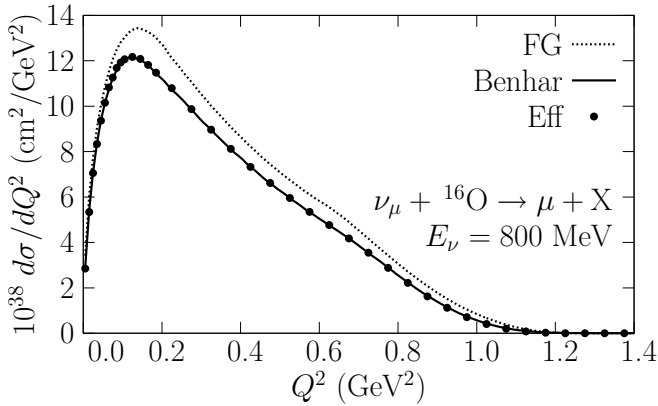

FIG. 13: Quasielastic differential cross section $d\sigma/dE_\mu$ of $^{40}_{18}$Ar obtained from the effective description, our spectral function and the Fermi gas ($p_F = 251$ MeV, $\overline{\epsilon}_B = 28$ MeV). Pauli blocking is present.

FIG. 12: Quasielastic differential cross section in $Q^2 = -q^2$ of ^{16}O obtained from the effective description, the Benhar's spectral function and the Fermi gas ($p_F = 225$ MeV, $\overline{\epsilon}_B$=27 MeV). Pauli blocking is present.

FIG. 14: Quasielastic differential cross section $d\sigma/d|\mathbf{p}'|$ of $^{40}_{18}$Ar obtained from the effective description, our spectral function and the Fermi gas ($p_F = 251$ MeV, $\overline{\epsilon}_B = 28$ MeV). Pauli blocking is absent.

description represents a major improvement over the FG model.

We compare also predictions of the three models for the distribution of nucleons ejected from oxygen. The results are shown in Fig. 11. In the computations we did not apply the Pauli blocking. Its straightforward implementation simply eliminates nucleons with momenta lower then the Fermi momentum. Predictions of the spectral function and the effective description are almost identical. It is because the distributions of momenta of two approaches are the same. We see again that the effective description is a good approximation of the spectral function.

As is shown in Fig. 12, the effective model also succeeds in precisely reproducing the SF's differential cross section $d\sigma/dQ^2$.

Finally in Figs. 13 and 14 we show a comparison of predictions from our spectral function of argon with the effective description based on it. The differences between
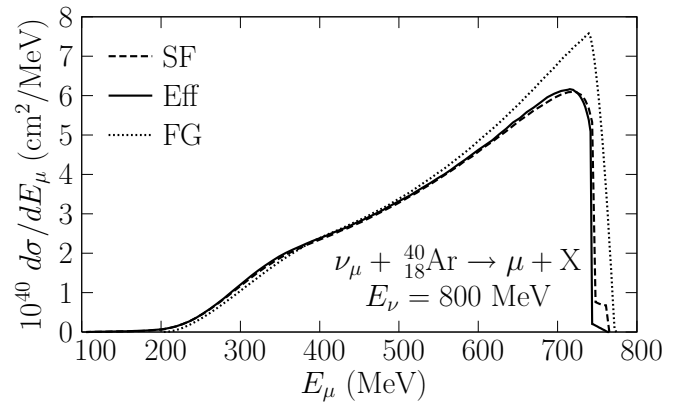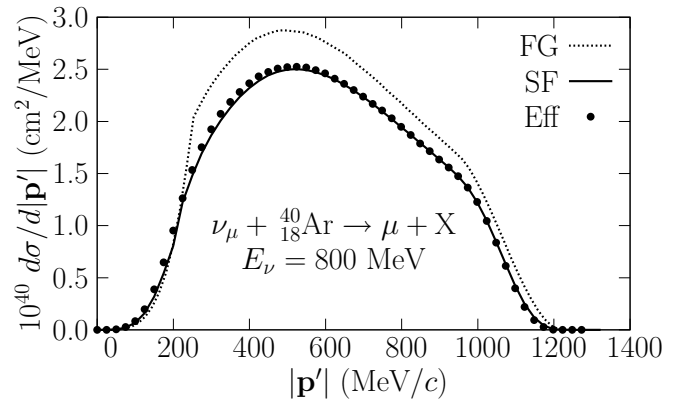
the two models are smaller then in the case of oxygen because of the way in which the dominant mean field part of the argon SF was treated. We notice that the singularity present in Fig. 13 caused by the treatment of isovector part of the spectral function is not seen in Fig 14.

IV. CONCLUSIONS

We constructed the spectral function for argon and applied it in the PWIA computation of the CC quasielastic cross section of neutrino-argon scattering. The construction method was based on the ideas contained in [22]. We verified that when applied to oxygen, the method leads to the results similar to those obtained from the more detailed spectral function obtained by Benhar [9]. The only FSI effect included in the discussion was Pauli blocking. We proposed also the effective approach in which the

information contained in the spectral function is used to define two functions. We argued that this approach yields results similar to the spectral function, but at the same time it can be easily applied in MC routines.

We see two possible applications of our results. The argon spectral function can be used in more precise computations of the neutrino cross sections in a few GeV energy region. The effective approach may be used in existing MC event generators giving rise to the important improvement with respect to the Fermi gas model. For example, Fig. 12 shows that it reconstructs well the Q^2 distribution of events which is important because of the observed low Q^2 deficit of events in the K2K experiment.

The effective approach can be also used in cross section computations for other targets important in neutrino experiments like carbon and iron for which appropriate SFs exist [37].

[1] *Proceedings of NuInt01*, edited by J.G. Morfin, M. Sakuda, and Y. Suzuki [Nucl. Phys. B (Proc. Suppl.) **112** (2002)]; *Proceedings of NuInt04*, edited by F. Cavanna, P. Lipari, C. Keppel and M. Sakuda [*ibid.* **139** (2005)].

[2] R.A. Smith and E.J. Moniz, [Erratum: *ibid.* **B101**, 547 (1975)].

[3] A. Bodek and J.L. Ritchie, Phys. Rev. D **23**, 1070 (1981).

[4] S.K. Singh and E. Oset, Phys. Rev. C **48**, 1246 (1993); T.S. Kosmas, E. Oset, Phys. Rev. C 53, 1409 (1996).

[5] S. Frullani and J. Mougey, Adv. Nucl. Phys. **14**, 1 (1984).

[6] C. Ciofi degli Atti and S. Simula, Phys. Rev. C **53**, 1689 (1996).

[7] O. Benhar, A. Fabrocini, S. Fantoni, and I. Sick, Nucl. Phys. **A579**, 493 (1994).

[8] D. Rohe et al. (E97-006 Collaboration), Phys. Rev. Lett. **93**, 182501 (2004); D. Rohe, for the E97-006 Collaboration, Nucl. Phys. B (Proc. Suppl.) **159**, 152 (2006).

[9] O. Benhar, N. Farina, H. Nakamura, M. Sakuda, and R. Seki, Phys. Rev. D **72**, 053005 (2005).

[10] O. Benhar, A. Fabrocini, S. Fantoni, G.A. Miller, V.R. Pandharipande, and I. Sick, Phys. Rev. C **44**, 2328 (1991); M. Petraki et al., Phys. Rev. C **67**, 014605 (2003); O. Benhar, Nucl. Phys. B (Proc. Suppl.) **159**, 168 (2006).

[11] T. Leitner, L. Alvarez-Ruso and U. Mosel, Phys. Rev. C **73**, 065502 (2006).

[12] J. Nieves, J. E. Amaro and M. Valverde, Phys. Rev. C**70**, 055503 (2004) [Erratum *ibid.* **72**, 019902 (2005)].

[13] C. Maieron, M.C. Martinez, J.A. Caballero, and J.M. Udias, Phys. Rev. C **68** (2003) 048501; C. Maieron, Acta Phys. Pol. B **37**, 2287 (2006).

[14] A. Meucci, F. Capuzzi, C. Giusti, and F.D. Pacati, Phys. Rev. C **67** 054601 (2003).

[15] J. Marteau, Eur. Phys. J. A **5**, 183 (1999); J.T. Sobczyk, "Modelling nuclear effects in neutrino interactions in 1 GeV region", arXiv:nucl-th/0307047.

[16] H. Nakamura and R. Seki, Nucl. Phys. B (Proc. Suppl.) **112**, 197 (2002); H. Nakamura, R. Seki, and M. Sakuda, *ibid.* **139**, 201 (2005).

[17] T. Sato, D. Uno, and T.-S. H. Lee, Phys. Rev. C **67**, 065201 (2003); T. Sato, B. Szczerbinska, K. Kubodera and T.-S. H. Lee, Nucl. Phys. B (Proc. Suppl.) **159**, 141 (2006).

[18] O. Lalakulich and E.A. Paschos, Phys. Rev. D **71**, 074003 (2005); O. Lalakulich, E. A. Paschos and G. Piranishvili, Phys. Rev. D **74**, 014009 (2006).

[19] O. Benhar and D. Meloni, Phys. Rev. Lett. (to be published).

[20] E. Oset, L.L. Salcedo, D. Strottman, Phys. Lett. **B165**, 13 (1985); E. Oset, L.L. Salcedo, Nucl. Phys. **A468**, 631 (1987).

[21] Z.A. Meziani et al., Phys. Rev. Lett. **54**, 1233 (1985)

[22] S.A. Kulagin and R. Petti, Nucl. Phys. **A765**, 126 (2006).

[23] T. de Forest, Jr., Nucl. Phys. **A392**, 232 (1983).

[24] O. Benhar, A. Fabrocini, and S. Fantoni, Nucl. Phys. **A505**, 267 (1989).

[25] A.M. Ankowski *et al.* (ICARUS Collaboration), Eur. Phys. J. C (to be published); J. Kisiel, Nucl. Phys. **B** (Proc. Suppl.) **155**, 205 (2006); S. Amerio et al. (ICARUS Collaboration), Nucl. Instrum. Meth. A **527**, 329 (2004); F. Arneodo et al. (ICARUS Collaboration), "The ICARUS Experiment...", arXiv:hep-ex/0103008.

[26] A. Meregaglia, Nucl. Phys. **B** (Proc. Suppl.) **155**, 248 (2006); S. Pordes, Nucl. Phys. **B** (Proc. Suppl.) **155**, 225 (2006); D. Finley et al., Fermilab: **FN-0776-E**.

[27] A. Meragaglia and A. Rubbia, Acta Phys. Pol. B **37**, 2387 (2006).

[28] C. Ciofi degli Atti, S. Liuti, and S. Simula, Phys. Rev. C **41**, R2474 (1990).

[29] C. Ciofi degli Atti, S. Simula, L.L. Frankfurt, and M.I. Strikman, Phys. Rev. C **44**, R7 (1991).

[30] G.A. Lalazissis, S.E. Massen, and C.P. Panos, Phys. Rev. C **48**, 944 (1993).

[31] V. Gillet, N. Vinh Mau, Nucl. Phys. **54**, 321 (1964).

[32] A. Bohr, B.R. Mottelson, *Nuclear Structure* (W.A. Benjamin Inc., New York, Amsterdam, 1969), Vol. 1, p. 232 and 326.

[33] C. Juszczak, J.A. Nowak, and J.T. Sobczyk, Eur. Phys. J. C **39**, 195 (2005).

[34] E.J. Moniz *et al.*, Phys. Rev. Lett. **26**, 445 (1971); R.R. Whitney *et al.*, Phys. Rev. **C9**, 2230 (1974), J. Engel, E. Kolbe, K. Langanke, P. Vogel, Phys. Rev. **D48**, 3048 (1993).

[35] W. Tornow, Z.P. Chen, and J.P. Delaroche, Phys. Rev. C **42**, 693 (1990).

[36] C.H. Johnson, C. Mahaux, Phys. Rev. C **38**, 2589 (1988).

[37] O. Benhar, private communication.